FULL PAPER

Dalton
www.rsc.org/dalton

The reaction of [Fe(pic)$_3$] with hydrogen peroxide: a UV-visible and EPR spectroscopic study (Hpic = picolinic acid)†

Sneh L. Jain* and Pravat Bhattacharyya

School of Chemistry, University of St Andrews, St Andrews, Fife, Scotland, UK KY16 9ST. E-mail: slj2@st-andrews.ac.uk; Fax: (+44)-1334-463808

Received 11th April 2005, Accepted 22nd June 2005
First published as an Advance Article on the web 7th July 2005

The Gif family of catalysts, based on an iron salt and O_2 or H_2O_2 in pyridine, allows the oxygenation of cyclic saturated hydrocarbons to ketones and alcohols under mild conditions. The reaction between [Fe(pic)$_3$] and hydrogen peroxide in pyridine under GoAgg^{III} (Fe(III)/Hpic catalyst) conditions was investigated by UV-visible spectrophotometry. Reactions were monitored at 430 and 520 nm over periods ranging from a few minutes to several hours at 20 °C. A number of kinetically stable intermediates were detected, and their relevance to the processes involved in the assembly of the active GoAgg^{III} catalyst was determined by measuring the kinetics in the presence and absence of cyclohexane. EPR measurements at 110 K using hydrogen peroxide and *t*-BuOOH as oxidants were used to further probe these intermediates. Our results indicate that in wet pyridine [Fe(pic)$_3$] undergoes reversible dissociation of one picolinate ligand, establishing an equilibrium with [Fe(pic)$_2$(py)(OH)]. Addition of aqueous hydrogen peroxide rapidly generates the high-spin complex [Fe(pic)$_2$(py)(η^1-OOH)] from the labilised hydroxy species. Subsequently the hydroperoxy species undergoes homolysis of the Fe–O bond, generating HOO$^{\bullet}$ and [Fe(pic)$_2$(py)$_2$], the active oxygenation catalyst.

Introduction

The catalytic functionalisation of C–H bonds in alkanes sustains extensive and ongoing interest worldwide, with systems mimicking the dioxygen activation induced by iron-containing biological systems such as bleomycin, cytochrome P450 and methane monooxygenase receiving particular attention.[1] One attractive group of catalysts for the oxygenation of cycloalkanes to ketones and alcohols is the Gif family of oxidants,[2–5] within which Gif^{IV} [a heterogeneous mixture of an iron(II) salt, dioxygen, acetic acid and zinc dust in pyridine] is the most efficient manifold, with turnover numbers for ketonisation exceeding 2000. The mechanism of Gif systems has, since their inception, provoked fierce debate; the current consensus of opinion favours a radical-based pathway, displacing Barton's original proposal of iron(V) oxo intermediates.[2,3]

The GoAgg^{III} system,[6,7] comprising an iron(III) salt, picolinic acid (Hpic) and aqueous hydrogen peroxide is a homogenous counterpart of Gif^{IV}. Hpic is a powerful promoter of Gif chemistry, far more so than other nitrogen-containing heteroaromatics, and the following observations are notable: (a) Hpic reduces the requirement for pyridine and affords a higher conversion rate; (b) the ideal ratio for efficient ketonisation of cycloalkanes is iron(III) : Hpic : hydrogen peroxide = 1 : 4 : 4; (c) with two equivalents of Hpic to iron salt, *in situ* dioxygen production (catalase activity) is suppressed.[8–10] Pyridine can largely be replaced by acetonitrile,[11] but cannot entirely be removed without substantial loss of catalytic activity. This reflects its importance in stabilising iron intermediates by coordination, as well as its involvement in the radical chemistry which underpins the Gif reaction. The use of GoAgg^{III} catalysis to selectively oxidise complex natural products underlines both the mildness and versatility of this system.[12–15]

Barton's investigations of GoAgg^{III} using quantitative ^{13}C NMR spectroscopy[8] confirmed an earlier result,[16] that the reaction between iron(III) hexahydrate chloride and Hpic in pyridine–acetic acid generates [Fe(pic)$_2$Cl$_2$]$^-$, mooted as the true precatalyst in GoAgg^{III}, rather than [Fe(pic)$_3$]. Barton's synthesis of [Fe(pic)$_2$Cl$_2$]$^-$ is difficult to reproduce under the reported conditions, although we have recently published a more efficient procedure.[17] Nevertheless [Fe(pic)$_3$] is readily prepared and functional in GoAgg^{III} catalysis. When hydrogen peroxide is added to [Fe(pic)$_3$] in pyridine, rapid formation ($t_{1/2} \approx 1$ min at 20 °C) of a purple solution occurs ($\lambda_{max} = 530$ nm, $\varepsilon \approx 1000$ M^{-1} cm^{-1}), characteristic for the ligand–metal charge-transfer absorption of a non-haem iron(III) hydroperoxy species.[18] That this species is the predominant complex in solution is consistent with the results from numerous studies on the interaction of hydrogen peroxide with iron(II) and iron(III) precursors, which show that formation of the hydroperoxy species is very facile.[18] Within Gif chemistry iron(III) hydroperoxy species are the likeliest source of the oxygen-based radicals mediating the oxidation process. Iron–hydroperoxy complexes have been characterised by a battery of spectroscopic techniques, but kinetic investigations of the processes leading to their formation and decomposition are rare. Herein we detail our kinetic studies on the construction and decay of the intermediates generated when aqueous hydrogen peroxide is added to [Fe(pic)$_3$] in pyridine.

Experimental

Reagents and solvents (Aldrich, AR grade) were used as supplied, synthetic and spectroscopic procedures were conducted under aerobic conditions. [Fe(pic)$_3$] was prepared in methanol from Hpic and iron(III) nitrate nonahydrate. Stock solutions of [Fe(pic)$_3$] in pyridine (0.5 mM) were protected from light and used within three days of preparation. After this time solutions darkened due to unidentified reactions and were unsuitable for kinetic studies. Aqueous 30% w/w hydrogen peroxide was found to be 9.46 M upon standardisation with cerium(III) sulfate or potassium permanganate solutions.[19] X-Band EPR spectra were recorded in 4 mm o.d. tubes on a Bruker EMX 10/12 spectrometer operating at 9.5 GHz with 100 kHz modulation. The absorbance of a 3.0 cm^3 aliquot of [Fe(pic)$_3$] solution over the range 300–900 nm with varying concentrations of hydrogen peroxide in 1 cm path length quartz cuvettes was measured at 20.0 ± 0.1 °C using a Shimadzu W-2101 PC UV-vis spectrophotometer and a thermostatically controlled Lauda RM6 water-bath.

† Electronic supplementary information (ESI) available: Tables S1 and S2: Kinetic data for the [Fe(pic)$_3$]–hydrogen peroxide system. Fig. S1: $k_{2(obs)}$ *vs.* [H_2O_2] plot. See http://dx.doi.org/10.1039/b504897d

DOI: 10.1039/b504897d

Kinetic runs, studied by conventional means under pseudo first-order conditions with >40 equivalents of hydrogen peroxide (0.016–0.124 M) over [Fe(pic)$_3$] (0.5 mM), were initiated by injection of 5–40 μl aliquots of hydrogen peroxide into the [Fe(pic)$_3$] solution placed in the thermostatted cuvettes. Data were averaged over two runs. The reaction of [Fe(pic)$_3$] with 165 equivalents of hydrogen peroxide was initially monitored at 5 °C in order to obtain time-resolved spectra at intervals of 2 min (Fig. 1). The yellow solution rapidly became dark brownish-purple (λ_{max} 530 nm), after 12 min a second process was evident, characterised by an isosbestic point at 520 nm. Thereafter a further rise in absorbance over the entire wavelength range characterised much slower changes, which at 20 °C were accompanied by evolution of dioxygen, resulting in a deep yellow–brown solution after 12 h. For the detailed kinetic study, 430 nm (significantly away from the isosbestic point) and 520 nm wavelengths were chosen for monitoring. A preliminary investigation revealed that the rapid initial changes surrounding the isosbestic point could be followed at 20 °C using time intervals of 2 s.

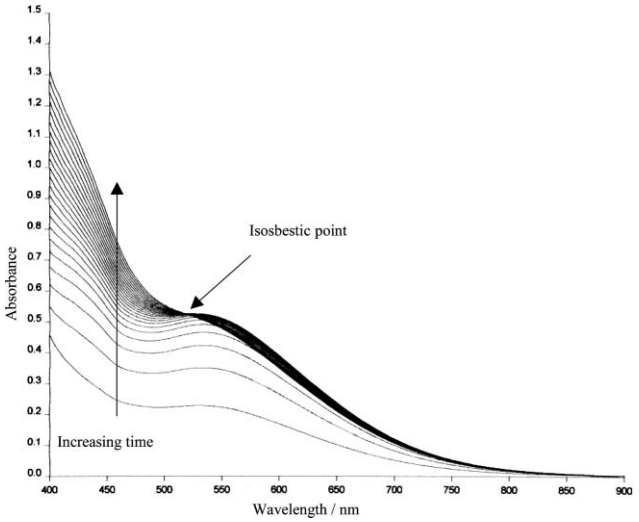

Fig. 1 Time-resolved spectra ($\Delta t = 2$ min) for [Fe(pic)$_3$] (0.5 mM) with 165 equivalents of hydrogen peroxide in pyridine at 5 °C.

Absorbance–time plots at 430 and 520 nm were fitted to either one or two successive exponentials using a non-linear least-squares fitting procedure provided by GRAFIT®.[20] For the fit to a single exponential, eqn. (1) was employed:

$$A_t = A[1 - \exp(-kt)] + A_0 \quad (1)$$

A_t is the absorbance at time t, A and k represent respectively the extent of absorbance change and rate constant for the single stage and A_0 is the absorbance at $t = 0$. For the fit to two exponentials, eqn. (2) was employed;

$$A_t = A_1[1 - \exp(-k_1 t)] + A_2[1 - \exp(-k_2 t)] + A_0 \quad (2)$$

A_1 and A_2 represent the extent of absorbance change for the first and second stages, respectively, k_1 and k_2 are the successive first-order rate constants. Since the end of the second stage is not fully defined due to subsequent reactions, evaluation of the parameters in eqn. (2) was achieved by first fixing values for A_1 and k_1 based on data gathered at 520 nm, wherein only the first stage contributes, and letting the program calculate values for A_2, k_2 and A_0 representing the best fit to the data (lowest value of χ^2). The fixed values of A_1 and k_1 were then each varied in succession until χ^2 was further minimised. These data appear in Tables S1 and S2 (ESI).†

Results and discussion

Kinetic measurements

The kinetics of the reaction of [Fe(pic)$_3$] with varying concentrations of hydrogen peroxide, in the absence or presence of cyclohexane (0.5 equivalents relative to hydrogen peroxide), were investigated at 20 °C. Absorbance–time plots as a function of [H_2O_2] at the isosbestic point (520 nm) over a 10 min period appear in Fig. 2. There is a delay of approximately 5 s between the addition of hydrogen peroxide and commencement of the spectroscopic measurement. The effect on A_0 is most pronounced at higher concentrations, however the intercept on the absorbance axis is not critical to the determination of the pseudo-first-order rate constant $k_{1(obs)}$.

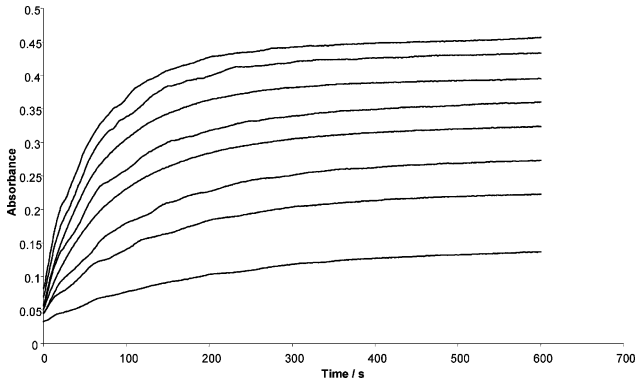

Fig. 2 Absorbance–time trace, [Fe] = 0.5 mM, [H_2O_2] = 0.016–0.124 M (20 °C, 520 nm). Increasing [H_2O_2] leads to higher absorbance.

The curves in Fig. 2 have first-order kinetic profiles over the first 10 min, from which $k_{1(obs)}$ for the formation of the initial iron(III) product can be calculated. In the presence of 0.5 equivalents of cyclohexane, absorbance–time traces at 520 nm when hydrogen peroxide was added showed the same characteristics (Fig. 3) *i.e.* the profiles were largely unaffected by addition of the hydrocarbon. The absorbance rise at 520 nm for runs with and without cyclohexane were fitted to the single exponential function [eqn. (1)], allowing $k_{1(obs)}$ to be obtained as a function of [H_2O_2] (Fig. 4). The extent of absorbance change increased with [H_2O_2], with evidence of saturation in A_∞ at higher concentrations. Taken together, these findings suggest a first-order reversible equilibration reaction [eqn. (3)] with the slope of the line in Fig. 4 characterising the forward rate constant (k_1) and the intercept, the rate constant for the reverse process (k_{-1}). Values of k_1 and k_{-1} in the presence and absence of cyclohexane (Table 1) demonstrate that adding the substrate during this stage of the reaction leads to some diminution of the rate (*ca.* 35%).

$$[\mathrm{Fe(pic)_3}] + \mathrm{H_2O_2} \underset{k_{-1}}{\overset{k_1}{\rightleftharpoons}} \mathbf{1}\,(\lambda_{max}530\,\mathrm{nm}) \quad (3)$$

During retention of the isosbestic point a second process is seen, which results in fading of the absorption maximum at 530 nm for the first intermediate to give a shoulder at *ca.* 500 nm

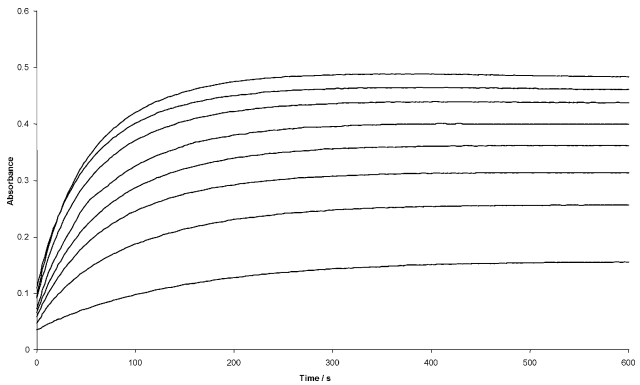

Fig. 3 Absorbance–time trace with cyclohexane (0.006–0.062 M) added: [Fe] = 0.5 mM, [H_2O_2] = 0.016–0.124 M (20 °C, 520 nm). Increasing [H_2O_2] leads to higher absorbance.

Table 1 Rate constants for [Fe(pic)$_3$]-hydrogen peroxide system

	Data collected at 520 nm		
Constant	Cyclohexane absent	Cyclohexane present	Data collected at 430 nm
k_1/M^{-1} s^{-1}	$(9.46 \pm 0.32) \times 10^{-2}$	$(8.08 \pm 0.69) \times 10^{-2}$	$(9.74 \pm 0.66) \times 10^{-2}$
k_{-1}/s^{-1}	$(3.59 \pm 0.24) \times 10^{-3}$	$(5.50 \pm 0.54) \times 10^{-3}$	$(4.39 \pm 0.52) \times 10^{-3}$
k_2/s^{-1}	—	—	$(1.00 \pm 0.05) \times 10^{-4}$

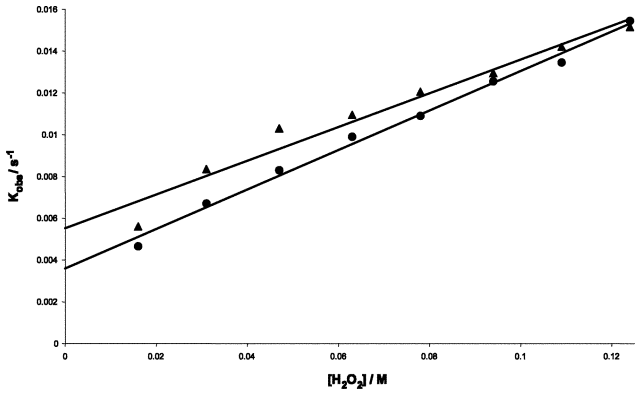

Fig. 4 k_{obs} *vs.* [H_2O_2] for the [Fe(pic)$_3$]–hydrogen peroxide system at 520 nm in the presence and absence of cyclohexane (triangles represent data with cyclohexane added, filled circles are data without cyclohexane).

and a general increase in the absorbance below 520 nm. To obtain data characterising this second process the reaction was monitored at 430 nm over 30 min with several hydrogen peroxide concentrations (Fig. 5). For each run a rapid rise over the first 2 min is followed by a slower increase over the next 10 min, subsequently the behaviour becomes more complex. The initial two stages could be fitted to two successive exponentials using eqn. (2). The first stage was found by the iterative treatment to correspond to the same process which resulted in the formation and retention of the isosbestic point. This evidence of a first-order equilibration was found to depend linearly on [H_2O_2]. The slower second process, however, was shown to be independent of [H_2O_2]. For both processes the extent of absorbance change (A_∞ value) increased with [H_2O_2] but showed evidence of saturation at higher concentrations. These are the classic hallmarks of equilibration processes. Rate constants $k_{2(obs)}$ obtained at 430 nm as a function of [H_2O_2] (Table S2, ESI†) clearly illustrate the independence of the second process on this concentration (Fig. S1, ESI†). Thus it can be concluded that the isosbestic point involves a further reaction taking place once the initial reaction with hydrogen peroxide is complete. Values for k_1 and k_{-1} (for the first stage leading to **1**) and k_2 (for the second stage leading to **2**) from the data obtained at 430 nm appear in Table 1. Our kinetic data are consistent with eqns. (3) and (4).

$$\mathbf{1} \overset{k_2}{\rightleftharpoons} \mathbf{2} \quad (4)$$

The k_2 value (1.0×10^{-4} s^{-1}) is smaller in magnitude than for the decomposition of iron(III) hydroperoxy complexes bearing 4,5-pinene-2,2′-bipy or *N*-methyl-*N*,*N*′,*N*′-tris(2-pyridylmethyl)propane-1,3-diamine co-ligands (2.0×10^{-3} s^{-1} at 0 °C in acetonitrile and 2.7×10^{-3} s^{-1} at 20 °C in methanol, respectively),[21,22] which are themselves consistent with k for the unimolecular decomposition of Fe^{III}–OOH in aqueous solution (2.7×10^{-3} s^{-1}).[23] For data collected in the absence of cyclohexane, k_1 (*ca.* 9×10^{-2} M^{-1} s^{-1}) is an order of magnitude smaller than for a similar system,[22] and contrasts markedly with values for the [Fe(pic)$_2$]–hydrogen peroxide reaction in pyridine–acetic acid (2.0×10^3 and 2.0×10^2 M^{-1} s^{-1} when the iron : H_2O_2 ratios are 1 : 1 and 1 : 200, respectively).[24] Our k_{-1} (*ca.* 4×10^{-3} s^{-1}) agrees with data for an iron(III) hydroperoxy complex with an *N*-benzyl-*N*,*N*′,*N*′-tris(2-pyridylmethyl)ethane-1,2-diamine ligand (5.0×10^{-3} s^{-1} at 20 °C).[25]

Talsi *et al.* have proposed that in pyridine K[Fe^{II}(pic)$_3$] irreversibly loses Hpic to form [Fe(pic)$_2$(OH)(py)].[26] To ascertain whether [Fe(pic)$_3$] underwent similar changes, runs were conducted in the presence of 10 equivalents of Hpic; should Hpic dissociation occur prior to rate-determining formation of **1**, a decrease in $k_{1(obs)}$ would be expected at each hydrogen peroxide concentration. The results (Fig. 6) show that the initial stage of the reaction clearly is much slower *cf.* Fig. 2, with the rate of the second stage largely unaffected. The effect of added Hpic upon the kinetics strongly suggests that [Fe(pic)$_3$] equilibrates with an iron(III)-bis(picolinate) complex, which by analogy with Talsi's work is likely to be [Fe(pic)$_2$(py)(OH)], formed by rapid pyridine/water (HO^-) coordination. This complex is a strong candidate for the species reacting with hydrogen peroxide in the rate-determining step to give **1** [eqns. (5) and (6)].

$$[\mathrm{Fe(pic)_3}] \overset{\mathrm{py,H_2O}}{\underset{K}{\rightleftharpoons}} [\mathrm{Fe(pic)_2(py)(OH)} + \mathrm{Hpic}] \quad (5)$$

$$[\mathrm{Fe(pic)_2(py)(OH)}] + \mathrm{H_2O_2} \overset{k_1}{\underset{k_{-1}}{\rightleftharpoons}} \mathbf{1} + \mathrm{H_2O} \quad (6)$$

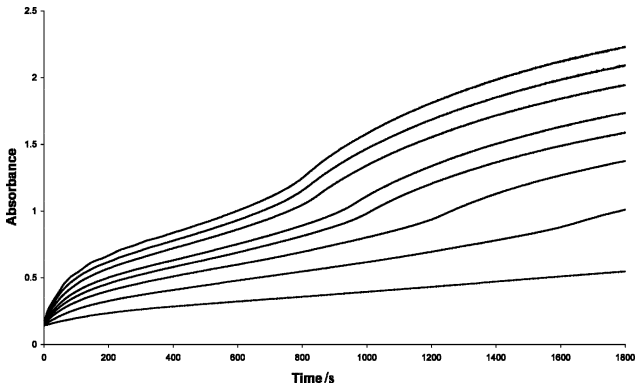

Fig. 5 Absorbance–time trace, [Fe] = 0.5 mM, [H_2O_2] = 0.016–0.124 M, (20 °C, 430 nm). Increasing [H_2O_2] leads to increased absorbance.

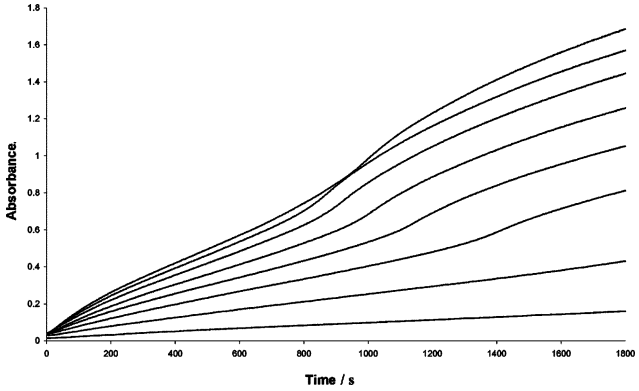

Fig. 6 Absorbance–time trace, [Fe] = 0.5 mM, [H_2O_2] = 0.016–0.124 M, with 10 equivalents of Hpic to iron (20 °C, 430 nm). Increasing [H_2O_2] leads to higher absorbance.

To establish whether the retardation induced by added Hpic was a general acid phenomenon, kinetic runs were performed with 10 equivalents of *p*-toluenesulfonic acid added to the solutions. A similar retardation occurred, albeit with a completely different absorbance–time profile, which could reflect protonation of the pyridine and suppression of its ability to displace Hpic in the initial step. Barton's quantitative ^{13}C NMR experiments showed that $[Fe(pic)_3]$ did not undergo Hpic dissociation in pyridine.[8]

EPR measurements (*vide infra*) confirm that upon dissolution of $[Fe(pic)_3]$ in pyridine chemical change occurs but that mononuclearity is retained *i.e.* there is no conversion into a μ-oxo bridged diferric complex. As the rate constants for the second stage of the reaction were independent of $[H_2O_2]$ and [Hpic], this implies the conversion of one bis(picolinate) complex **1** to another **2**. The saturation in A_∞ as $[H_2O_2]$ increases (Table S1, ESI†) indicates that this reaction, as with the first stage, is reversible. The A_∞ values for the second stage are, however, only estimates since after 10–30 min subsequent reactions occur, whose onset is dependent on $[H_2O_2]$.

When the reaction time exceeds 30 min a complex series of reactions occurs, shown in Fig. 7 for $[H_2O_2] = 0.042$ and 0.126 M with cyclohexane present and absent. At each concentration of hydrogen peroxide, the addition of cyclohexane, added prior to the H_2O_2, markedly decreased the overall absorbance during a 10 h period. The rate reduction upon cyclohexane addition indicates that the substrate reacts with the species responsible for the absorbance at this time. After approximately 6 h the curves for the 0.042 M runs intersect the traces for the 0.126 M aliquots, which reach a plateau after 3–4 h, leading to higher absorbances for the former. We infer that there may be precipitation of very minor quantities of iron(III) hydroxy species at the higher peroxide concentration, although we have obtained no direct evidence for this [*n.b.* formation of iron(III) oxide/hydroxide particles was observed by Schuchardt[27] during $GoAgg^{III}$ cyclohexane oxygenation]. Indeed, for the 0.042 M solution, the absorbance continues to rise steadily, even after 10 h, due to further reactions of the more soluble iron species.

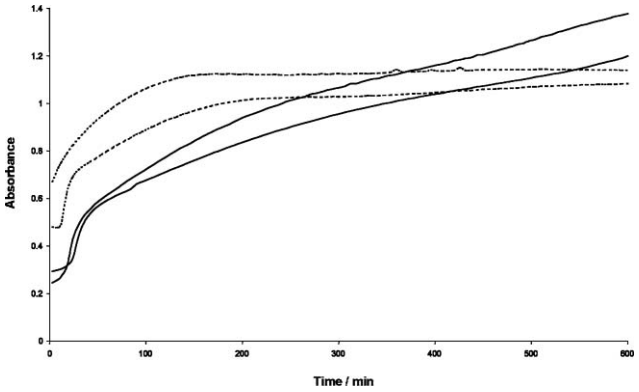

Fig. 7 Absorbance–time trace, [Fe] = 0.5 mM, $[H_2O_2] = 0.042$ and 0.126 M (20 °C, 520 nm). Dotted line = 0.126 M, full line = 0.042 M. Within each pair of curves the lower line represents when cyclohexane is added.

Scheme 1 summarises the reaction of $[Fe(pic)_3]$ with hydrogen peroxide in pyridine.

EPR Analysis

Talsi *et al.* used EPR and ^1H NMR spectroscopies to analyse the $K[Fe^{II}(pic)_3]$–hydrogen peroxide system;[26] in their study $[Fe^{III}(pic)_2(OH)(py)]$ ($g = 4.25$) was produced when 1 equivalent of hydrogen peroxide was added to a 2 : 1 v/v pyridine–acetic acid solution of $K[Fe(pic)_3]$. Addition of a large excess of hydrogen peroxide generated a high-spin iron(III) hydroperoxo complex, purportedly $[Fe(pic)_2(py)(OOH)]$. However no EPR study has been made of the corresponding reaction with $[Fe(pic)_3]$.

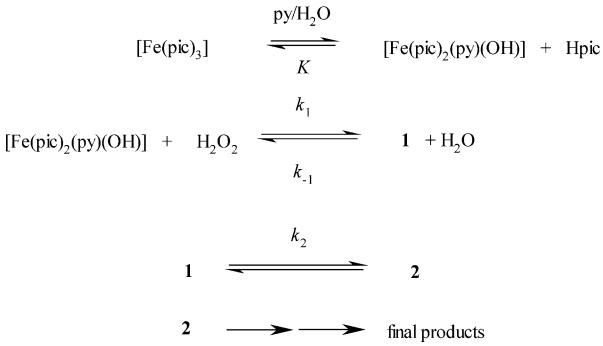

Scheme 1

To parallel our UV-vis study, an approximately 0.3 cm^3 aliquot was taken from 3.0 cm^3 of $[Fe(pic)_3]$ in pyridine (0.5 mM), transferred to an EPR tube and dipped into a vessel containing 5 : 1 v/v isopentane–methylcyclohexane, itself immersed in liquid nitrogen. This rapid freezing technique produced more clearly resolved spectra compared to when solely liquid nitrogen was used for cooling. The frozen solution was transferred to the spectrometer, whose cavity was maintained at 110 K. The X-band spectrum of the frozen glass showed a signal at $g = 4.4$ (Fig. 8(a)), compatible with the $m_s = \pm 1/2$ Kramers doublet of a high-spin ($S = 5/2$) iron(III) centre in a rhombically distorted environment, both in zero-field splitting (ZFS) and geometry. The rhombicity arises from the mixed ligands and the constraints imposed through the chelate effect with the picolinates. The complexity of the spectrum suggests that several isomeric high-spin species are formed, conceivably arising from reactions of $[Fe(pic)_3]$ with pyridine or water involving reversible loss of pic^-, consistent with eqn. (5) ($K \gg 1$).

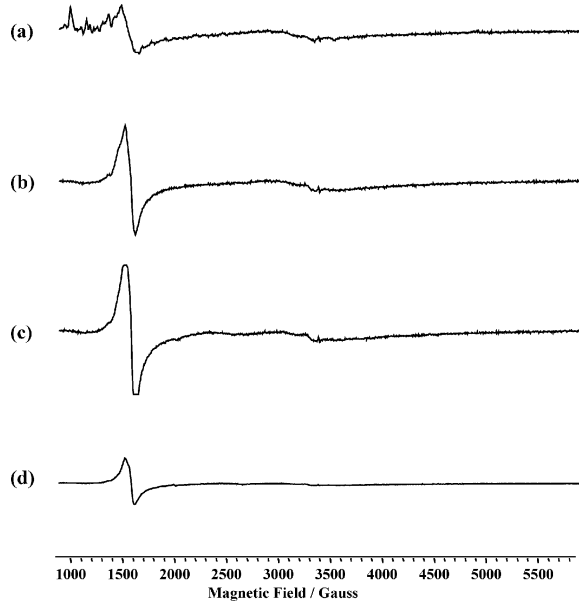

Fig. 8 X-Band EPR spectra at 110 K for (a) 0.5 mM solution of $[Fe(pic)_3]$ in pyridine. (b) Solution (a) with 170 equivalents of hydrogen peroxide after 2 min (purple species) at room temperature then refrozen. (c) Solution (b) warmed for a further 2 min and refrozen. (d) Solution (c) warmed for a further 2 min and refrozen. All spectra are shown to the same scaling along the absorbance axis.

The EPR tube was removed from the spectrometer, thawed completely and its contents combined with the stock solution. An aliquot of hydrogen peroxide (20 μl, *ca.* 170 equivalents over iron) was added, giving a purple colour. After 2 min a portion of the solution was transferred into a clean tube, frozen as before and its EPR spectrum recorded (Fig. 8(b)). An isotropic $g = 4.4$ signal appeared, whose sharpness and intensity suggests an increase in molecular symmetry in the

oxidised complex compared to [Fe(pic)$_3$] and the presence of a single major high-spin component. The appearance of only one resonance upon hydrogen peroxide addition is consistent with several related studies into the formation of iron–hydroperoxy intermediate.[18] Two consecutive cycles of removal from the spectrometer, thawing for 2 min and refreezing (Fig. 8(c) and (d)) suggest an initial increase and subsequent decrease in the $g = 4.4$ signal, however double integration gave inaccurate values of signal intensity as the baselines were insufficiently flat. In Fig. 8(b) and (c) a low-field shoulder at the main signal arises from the rhombicity parameter $\lambda \approx 0.17$ ($\lambda = E/D$, where D and E are the axial and rhombic ZFS parameters, respectively) rather than $\lambda = 1/3$, which is the maximum possible rhombicity in ZFS. Whereas iron(III) hydroperoxy complexes bearing polydentate aminopyridyl co-ligands are exclusively low-spin,[18] the more oxygen-rich environment about the iron core in **1** favours a high-spin configuration, only the second such example,[28] which has important ramifications for its subsequent reactivity (*vide infra*).

Further clues to the nature of **2** (and hence **1**) came from EPR studies of the reaction of [Fe(pic)$_3$] in pyridine with *t*-BuOOH, a reagent which can replace hydrogen peroxide in Gif (GoAgg) chemistry and preserve the main reactivity profile. The [Fe(pic)$_3$]–*t*-BuOOH reaction was studied under analogous conditions to the hydrogen peroxide experiment, *i.e.* with 170 equivalents of hydroperoxide. A deep purple solution forms rapidly at 20 °C upon *t*-BuOOH addition to [Fe(pic)$_3$]. The $g = 2$ signal in the EPR spectrum of the frozen glass after 2 min of reaction (Fig. 9(b)) is due to *t*-BuOO$^{\bullet}$, consistent with Fe–O cleavage of [Fe(pic)$_2$(py)(OOBu-*t*)], producing the EPR-silent high-spin iron(II) complex [Fe(pic)$_2$(py)$_2$]. The assignment is supported by the observations that treatment of [Fe(pic)$_3$] with hydrogen peroxide generates [Fe(pic)$_2$(py)$_2$],[29] and that K[Fe(pic)$_3$] converts into [Fe(pic)$_2$(py)$_2$] when dissolved in pyridine.[26] The EPR silence of the complex arises from the large ZFS, causing the potentially allowed transitions to be at too high an energy to be excited by X-band microwave frequency. Further corroboration is provided by Que's findings that the Fe–O bond cleaves in high-spin iron(III) butylperoxyl complexes with 6-methyl substituted tris(2-pyridylmethyl)amine ligands, whereas O–O homolysis occurs in low-spin analogues.[30] The g value for the iron(III) butylperoxyl species in Fig. 9(b) is consistent with Que's high-spin complexes ($g = 4.3$),[31] although such nitrogen-rich coordination environments typically favour low-spin configurations.[32–34] As in Fig. 8, the feature to low-field of the $g = 4.4$ signal could belong to the main absorption with differences in the ZFS parameters, though still with significant rhombicity.

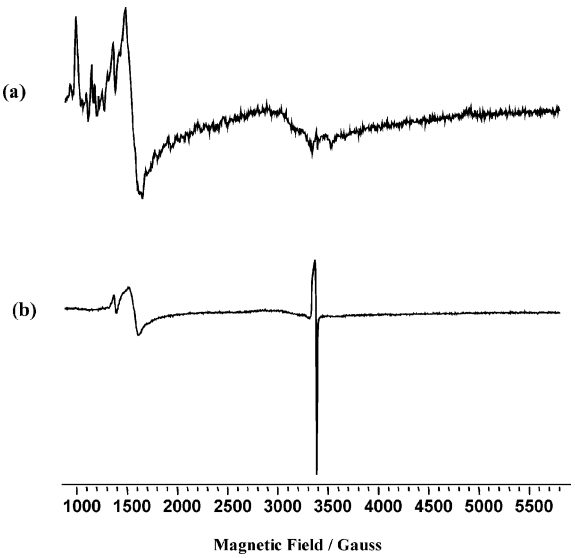

Fig. 9 X-Band EPR spectra at 110 K for (a) 0.5 mM solution of [Fe(pic)$_3$] in pyridine. (b) Solution (a) with 170 equivalents of *t*-BuOOH after 2 min (purple species) at room temperature then refrozen.

Since *t*-BuOOH and hydrogen peroxide give similar purple species it is concluded, by extrapolation, that in the latter reactions **1** is the iron(III) hydroperoxy complex [Fe(pic)$_2$(py)(OOH)] and **2** is [Fe(pic)$_2$(py)$_2$] along with HOO$^{\bullet}$; this radical species, unlike *t*-BuOO$^{\bullet}$, has a short half-life in these solutions and rapidly disproportionates to hydrogen peroxide and dioxygen. Indeed the evolution of dioxygen is a feature of these solutions as they warm to room temperature over several minutes. Furthermore, despite the basicity of the solvent, we exclude the possibility of an Fe(η^2-O$_2$) or Fe$_2$(μ-O$_2$) structure for **1**, as the EPR of the *t*-BuOOH reaction was essentially identical to the H_2O_2 study.

Summary and conclusions

Barton has written that "... the hydrocarbon oxidation mechanisms of, say, Fe(PA)$_3$ [PA = picolinate] compared with FeCl$_3$·6H$_2$O + three picolinic acid could be different, as they differ in their starting materials...".[10] Although it is difficult to disagree with this statement, some similarities are evident. Since [Fe(pic)$_3$] is readily synthesised and does catalyse cycloalkane oxygenation under GoAgg^{III}, we undertook a kinetic study of its chemistry with hydrogen peroxide.

The [Fe(pic)$_3$]–hydrogen peroxide reaction in pyridine was monitored using UV-vis and EPR spectroscopies. Upon dissolution of [Fe(pic)$_3$] in non-dried pyridine, an equilibrium reaction involving displacement of one picolinate ligand by solvent and HO$^-$/H$_2$O is suggested by the dependence of the kinetics on added Hpic. On addition of aqueous hydrogen peroxide the formation of a hydroperoxy complex **1** takes place, followed by a slower transformation, the generation of the active catalyst **2** from **1**. The rate constants for the formation and subsequent reactions of **1** or **2** are typically smaller than in iron(III) hydroperoxy complexes with polyamine ligands, due to the *N*,*O*-donor environment. Over longer timeframes the presence of cyclohexane dramatically affects the absorbance of the solution, as **2** catalyses the oxygenation of the substrate. The EPR spectrum of [Fe(pic)$_3$] in pyridine at 110 K contains a complex signal at $g = 4.4$, consistent with equilibration mixtures of high-spin tris- and bis-(picolinate) iron(III) species, as detected in our kinetic studies. The production of an isotropic signal at $g = 4.4$ on reaction with hydrogen peroxide reflects the presence of a single high-spin complex, the decrease of signal intensity with time signifying conversion to an EPR-silent $S = 2$ component. *t*-BuOOH gives almost identical spectra under these conditions, suggesting that similar high-spin Fe^{III}–OOR (R = H or *t*-Bu) complexes are formed. We conclude that **1** and **2** are [Fe(pic)$_2$(py)(η^1-OOH)] and [Fe(pic)$_2$(py)$_2$], respectively. It is feasible that pyridine could deprotonate the hydroperoxy complex to give [Fe(pic)$_2$(η^2-O$_2$)]$^-$,[16] particularly as iron(III) peroxo complexes are high-spin,[18,35,36] moreover η^1-hydroperoxo ↔ η^2-peroxo interconversions can be effected by acid/base introduction.[25,37] However, the similarity between the hydrogen peroxide and *t*-BuOOH EPR experiments firmly refute that deprotonation is occurring. That Fe–O bond cleavage occurs in our high-spin Fe^{III}–OOR species (R = H or *t*-Bu) mitigates against the formation of high-valent iron–oxo intermediates in GoAgg^{III} oxidation using [Fe(pic)$_3$], although such species are readily invoked from low-spin precursors.

The formation of iron(II) species prior to any detectable influence of added cyclohexane accords with the current body of opinion, that Fenton/Haber–Weiss reactions involving radical formation from iron(II)–hydrogen peroxide chemistry underpins the mechanism of oxygenation by Gif systems. The involvement of pyridine in stabilising bis(picolinate) intermediates in addition to intercepting HO$^{\bullet}$ makes it an integral component of the Gif (GoAgg) protocol.

Acknowledgements

We acknowledge Dr W. John Ingledew, Dr Rona R. Ramsay and Prof. John C. Walton (University of St Andrews) for assistance with spectrometric measurements. We thank the EPSRC (P. B.) and BBSRC (S. L. J.) for financial support and Dr David Collison (The University of Manchester) for very helpful discussions.

References

1 M. Costas, M. P. Mehn, M. P. Jensen and L. Que, *Chem. Rev.*, 2004, **104**, 939.
2 P. Stavropoulos, R. Çelenligil-Çetin and A. E. Tapper, *Acc. Chem. Res.*, 2001, **34**, 745.
3 F. Gozzo, *J. Mol. Catal. A*, 2001, **171**, 1.
4 D. H. R. Barton, *Tetrahedron*, 1998, **54**, 5805.
5 D. H. R. Barton and D. Doller, *Acc. Chem. Res.*, 1992, **25**, 504.
6 D. H. R. Barton, E. Csuhai and D. Doller, *Tetrahedron Lett.*, 1992, **33**, 3413.
7 D. H. R. Barton, B. Hu, D. K. Taylor and R. U. R. Wahl, *Tetrahedron Lett.*, 1996, **37**, 1133.
8 D. H. R. Barton, B. Hu, R. U. R. Wahl and D. K. Taylor, *New. J. Chem.*, 1996, **20**, 121.
9 E. About-Jaudet, D. H. R. Barton, E. Csuhai and N. Ozbalik, *Tetrahedron Lett.*, 1990, **31**, 1657.
10 D. H. R. Barton, B. Hu, D. K. Taylor and R. U. R. Wahl, *J. Chem. Soc., Perkin Trans. 2*, 1996, 1031.
11 D. H. R. Barton and T. Li, *Tetrahedron*, 1998, **54**, 1735.
12 D. Doller, S. Chackalamannil, A. Stamford, B. McKittrick and M. Czarniecki, *Bioorg. Med. Chem. Lett.*, 1997, **7**, 1381.
13 D. H. R. Barton and D. Doller, *Collect. Czech. Chem. Commun.*, 1991, **56**, 984.
14 I. Okamoto, W. Funaki, K. Nakaya, E. Kotani and T. Takeya, *Chem. Pharm. Bull.*, 2004, **52**, 756.
15 S. B. Kim, K. W. Lee, Y. J. Kim and S. I. Hong, *Bull. Korean Chem. Soc.*, 1994, **15**, 424.
16 D. H. R. Barton, S. D. Beviere, W. Chavisiri, D. Doller, G. Liu and J. H. Riebenspies, *New J. Chem.*, 1992, **16**, 1019.
17 S. L. Jain, P. Bhattacharyya, H. L. Milton, A. M. Z. Slawin and J. D. Woollins, *Inorg. Chem. Commun.*, 2004, **7**, 423.
18 J. J. Girerd, F. Banse and A. J. Simaan, *Struct. Bonding (Berlin)*, 2000, **97**, 146.
19 A. I. Vogel, *Textbook of Quantitative Inorganic Analysis*, Longman, London and New York, 4th edn., 1978.
20 GRAFIT® is a trademark of Erithacus Software, Leatherhead, Surrey, UK. The package uses a standard Marquardt algorithm for non-linear least-squares fitting.
21 Y. Mekmouche, H. Hummel, R. Y. N. Ho, L. Que, V. Schünemann, F. Thomas, A. X. Trautwein, C. Lebrun, K. Gorgy, J.-C. Leprêtre, M.-N. Collomb, A. Deronzier, M. Fontecave and S. Ménage, *Chem. Eur. J.*, 2002, 1196.
22 V. Balland, F. Banse, E. Anxolabéhère-Mallart, M. Ghiladi, T. A. Mattioli, C. Philouze, G. Blondin and J. J. Girerd, *Inorg. Chem.*, 2003, **42**, 2470.
23 J. DeLaat and H. Gallard, *Environ. Sci. Technol.*, 1999, **33**, 2726.
24 C. Sheu, S. A. Richert, P. Cofré, B. Ross, A. Sobkowiak, D. T. Sawyer and J. R. Kanofsky, *J. Am. Chem. Soc.*, 1990, **112**, 1936.
25 A. Hazell, C. J. McKenzie, L. P. Nielsen, S. Schindler and M. Wietzer, *J. Chem. Soc., Dalton Trans.*, 2002, 310.
26 A. P. Sobolev, D. E. Babushkin, A. A. Shubin and E. P. Talsi, *J. Mol. Catal. A*, 1996, **112**, 253.
27 U. Schuchardt, C. E. Z. Krähembühl and W. A. Carvalho, *Stud. Surf. Sci. Catal.*, 1994, **82**, 647.
28 A. Wada, S. Ogo, S. Nagamoto, T. Kitagawa, Y. Watanabe, K. Jitsukawa and H. Masuda, *Inorg. Chem.*, 2002, **41**, 616.
29 S. Kiani, A. Tapper, R. J. Staples and P. Stavropoulos, *J. Am. Chem. Soc.*, 2000, **122**, 7503.
30 N. Lehnert, R. Y. N. Ho, L. Que and E. I. Solomon, *J. Am. Chem. Soc.*, 2001, **123**, 12802.
31 Y. Zang, J. Kim, Y. Dong, E. C. Wilkinson, E. H. Appelman and L. Que, *J. Am. Chem. Soc.*, 1997, **119**, 4197.
32 M. Rivera, G. A. Caignan, A. V. Astashkin, A. M. Raitsimring, T. K. Shokhireva and F. A. Walker, *J. Am. Chem. Soc*, 2002, **124**, 6077.
33 A. P. Sobolev, D. E. Babushkin and E. P. Talsi, *J. Mol. Catal. A*, 2000, **159**, 233.
34 M. V. Lobanova, K. P. Bryliakov, E. A. Duban and E. P. Talsi, *Mendeleev Commun.*, 2003, 175.
35 O. Horner, C. Jeandey, J. L. Oddou, P. Bonville, C. J. McKenzie and J. M. Latour, *Eur. J. Inorg. Chem.*, 2002, 3278.
36 A. J. Simaan, F. Banse, J. J. Girerd, K. Wieghardt and E. Bill, *Inorg. Chem.*, 2001, **40**, 6538.
37 K. B. Jensen, C. J. McKenzie, L. P. Nielsen, J. Z. Pedersen and H. M. Svendsen, *Chem. Commun.*, 1999, 1313.